



## Sound velocities of hydrous ringwoodite to 16 GPa and 673 K

Zhu Mao <sup>a,\*</sup>, Jung-Fu Lin <sup>a</sup>, Steven D. Jacobsen <sup>b</sup>, Thomas S. Duffy <sup>c</sup>, Yun-Yuan Chang <sup>b</sup>, Joseph R. Smyth <sup>d</sup>, Daniel J. Frost <sup>e</sup>, Erik H. Hauri <sup>f</sup>, Vitali B. Prakapenka <sup>g</sup>

<sup>a</sup> Department of Geological Sciences, Jackson School of Geosciences, The University of Texas at Austin, Austin, TX 78712, USA

<sup>b</sup> Department of Earth and Planetary Sciences, Northwestern University, Evanston, IL 60208, USA

<sup>c</sup> Department of Geosciences, Princeton University, Princeton, NJ 08544, USA

<sup>d</sup> Department of Geological Sciences, University of Colorado, Boulder, CO 80309, USA

<sup>e</sup> Bayerisches Geoinstitut, Universität Bayreuth, D-95440 Bayreuth, Germany

<sup>f</sup> Department of Terrestrial Magnetism, Carnegie Institution of Washington, Washington, DC 20015, USA

<sup>g</sup> Center for Advanced Radiation Sources, University of Chicago, Chicago, IL, USA

### ARTICLE INFO

#### Article history:

Received 4 November 2011

Received in revised form 10 February 2012

Accepted 2 March 2012

Available online xxxx

Editor: L. Stixrude

#### Keywords:

hydrous ringwoodite  
single-crystal elasticity  
high pressure-temperature  
Brillouin scattering

### ABSTRACT

To understand the effect of hydration on the sound velocities of major mantle minerals and to constrain the mantle's H<sub>2</sub>O budget, we have measured the single-crystal elastic moduli of hydrous ringwoodite, (Mg<sub>1.633</sub>Fe<sup>2+</sup><sub>0.231</sub>Fe<sup>3+</sup><sub>0.026</sub>)Si<sub>1.00</sub>H<sub>0.179</sub>O<sub>4</sub> with 1.1 wt.% H<sub>2</sub>O using Brillouin scattering combined with X-ray diffraction in an externally-heated diamond anvil cell up to 16 GPa and 673 K. Up to 12 GPa at 300 K, the presence of 1.1 wt.% H<sub>2</sub>O lowers the elastic moduli of ringwoodite by 5–9%, but does not affect the pressure derivatives of the elastic moduli compared to anhydrous ringwoodite. The reduction caused by hydration is significantly enhanced when temperatures are elevated at high pressures. At 12 GPa, increasing temperature by  $\Delta T = 100$  K leads to a 1.3–2.4% reduction in the elastic moduli ( $C_{11}$ ,  $C_{12}$ , and  $C_{14}$ ). Comparing our results with seismic observations, we have evaluated the potential H<sub>2</sub>O content in the lower part of the transition zone. Our results indicate that the observed seismic velocity anomalies and related depth depression of the 660-km discontinuity could be attributed to thermal variations together with the presence of ~0.1 wt.% H<sub>2</sub>O.

© 2012 Elsevier B.V. All rights reserved.

### 1. Introduction

Earth's mantle transition zone from 410 to 660-km depth exhibits seismic signatures reflecting thermo-chemical perturbations (e.g. Bina and Helffrich, 1994), including displaced depths of the nominal 410-km and 660-km discontinuities (e.g. Braunmiller et al., 2006; Courtier and Revenaugh, 2006; Niu et al., 2005; Tono et al., 2005), the depth interval of the 410-km discontinuity (e.g. Frost and Dolejš, 2007; Jasbinsek et al., 2010; van der Meijde et al., 2003), as well as lateral velocity variations compared to reference models (e.g. Courtier and Revenaugh, 2007; Nolet and Zielhuis, 1994; Song et al., 2004; van der Meijde et al., 2003). Observed anomalies have been proposed to correlate with the possible presence of H<sub>2</sub>O and thermal effects because the basaltic layer of cold subducted slabs may transport H<sub>2</sub>O to the transition zone (e.g. Ohtani, 2005; Smyth, 1987; Song et al., 2004; van der Meijde et al., 2003; Williams and Hemley, 2001).

The recent detection of a metastable olivine wedge within the slab beneath southwest Japan (Kawakatsu and Yoshioka, 2011) suggests that the slab interior is sufficiently dry (<100 ppm H<sub>2</sub>O) to depress the olivine–wadsleyite transition below 410 km. Transport of H<sub>2</sub>O in

minerals into the upper mantle thus more likely occurs along the upper few km of slabs (e.g. Kawakatsu and Watada, 2007). A lack of correlation between slab seismicity and known dehydration reactions below about 250-km depth (Green et al., 2010) has been used to suggest that negligible amount of water is transported into the transition zone, but this could also reflect changes in the rheology and water storage capacity of the nominally anhydrous phases at high pressures and temperatures. It is important to ask how much H<sub>2</sub>O is relevant to geophysical processes and geochemical cycling. Just one-tenth of a percent by weight H<sub>2</sub>O (1000 ppm wt) in the olivine–polymorphs of the transition zone would amount to a large mass fraction (~20%) of Earth's surficial H<sub>2</sub>O budget and be able to alter phase relations and reduce moduli. Therefore it is critical to accurately measure the influence of hydration on the equations of state of deep-mantle minerals at simultaneous high pressures and temperatures.

Due to the large water storage capacity of wadsleyite and ringwoodite, Earth's transition zone has the potential to accommodate several ocean's masses of H<sub>2</sub>O and contribute on geologic time scales to Earth's global water cycle (e.g. Bercovici and Karato, 2003; Hirschmann, 2006; Ohtani, 2005; Smyth and Jacobsen, 2006). The presence of H<sub>2</sub>O and associated defects in nominally anhydrous minerals have been shown to influence a number of physical properties, including electrical conductivity (e.g. Huang et al., 2005; Yoshino et al., 2008), elasticity (e.g. Jacobsen, 2004; Jacobsen, 2006; Jacobsen

\* Corresponding author.

et al., 2008; Mao et al., 2008a,b, 2010, 2011; Wang et al., 2003, 2006), and rheological and transport properties (e.g. Chen et al., 1998; Karato, 1995). Constraining the H<sub>2</sub>O content and identifying the potential H<sub>2</sub>O-rich region in the transition zone thus has potential implications for global mantle geochemistry, geophysics, and geodynamics.

The H<sub>2</sub>O content in the Earth's transition zone can be estimated by comparing the sound velocities of candidate hydrous minerals such as wadsleyite and ringwoodite with seismic velocities. Previous experiments at 300 K and first principle studies (at 0 K) have determined the high-pressure elasticity of hydrated transition zone minerals (Jacobsen and Smyth, 2006; Lin et al., 2009; Mao et al., 2008a,b, 2011; Tsuchiya and Tsuchiya, 2009; Wang et al., 2003, 2006). Using 300-K elastic properties and assuming no change in the temperature derivatives of moduli for hydrated phases requires a significant amount of H<sub>2</sub>O to explain the observed seismic velocity anomalies in the transition zone (e.g. Fukao et al., 2009; Suetsugu et al., 2006, 2010). Estimates from electrical conductivity and other seismic studies suggest lower H<sub>2</sub>O contents for the region (Green et al., 2010; Huang et al., 2005; Kelbert et al., 2009; Yoshino et al., 2008). As one of the most abundant phases in the transition zone, ringwoodite can incorporate more than 1 wt.% H<sub>2</sub>O at pressure–temperature (P–T) conditions relevant to the region (Inoue et al., 2010; Kohlstedt et al., 1996). Precise measurements on the elasticity of hydrous minerals at simultaneously high P–T conditions are needed to provide reliable constraints on the water content in the transition zone.

In this study, we have determined single-crystal elasticity of an Fe-bearing (Fe<sub>90</sub> composition) ringwoodite with 1.1 wt.% H<sub>2</sub>O at high P–T conditions using Brillouin spectroscopy and X-ray diffraction. The combined effects of hydration, pressure, and temperature on the elastic properties of ringwoodite are evaluated in terms of the potential seismic signature of hydration in the transition zone and used to infer the possible H<sub>2</sub>O content in the region. These results can be applied to better understand global H<sub>2</sub>O circulation and help to constrain the water budget in the Earth's deep interior.

## 2. Experimental details

Single-crystals of hydrous ringwoodite used in this study were synthesized at 18 GPa and 1400 °C in the 5000 ton press at

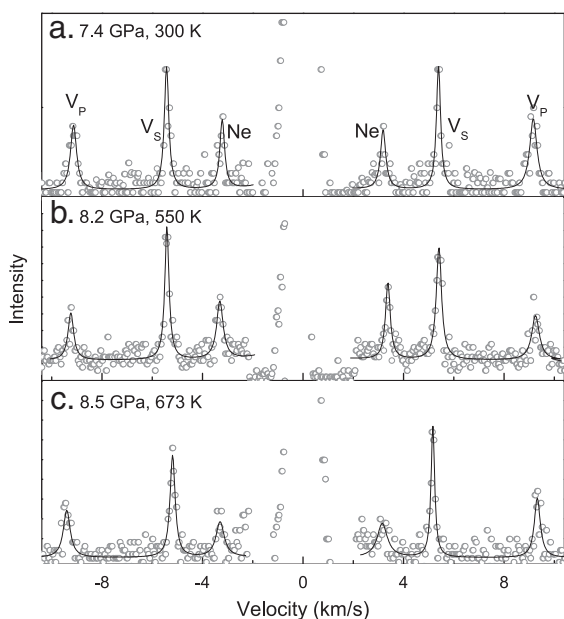


**Fig. 1.** Example of the measured Brillouin spectra compared with fitting results. Open circles: measurements; solid lines: fitting results. The uncertainty of the pressure is  $\pm 0.3$  GPa.

Bayerisches Geoinstitut, run number SZ0104 (Smyth et al., 2003). The previous study by Smyth et al. (2003) characterized the samples by electron microprobe, single-crystal X-ray diffraction, and Mössbauer spectroscopy. Here we include new high-precision lattice parameters by single-crystal X-ray diffraction and measured H<sub>2</sub>O content by secondary ion mass spectrometry (SIMS). Single-crystal X-ray diffraction using the eight-position centering method (King and Finger, 1979), which has allowed us to improve the precision of the lattice parameters measured previously (Smyth et al., 2003), yields a lattice parameter,  $a = 8.1060 (\pm 0.0007) \text{ \AA}$ , with a cell volume of  $532.62 (\pm 0.14) \text{ \AA}^3$ . The difference in lattice parameter between this study and Smyth et al. (2003) is within the experimental errors. The  $\text{Fe}^{3+}/\sum \text{Fe}$  ratio, measured by Mössbauer spectroscopy, is about 0.10 (Smyth et al., 2003). The water content of the ringwoodite sample was determined on the Cameca nanoSIMS 50L at the Department of Terrestrial Magnetism, Carnegie Institution of Washington. Using a 1 nA Cs<sup>+</sup> primary beam, a 10  $\mu\text{m}$  pre-sputter raster was carried out

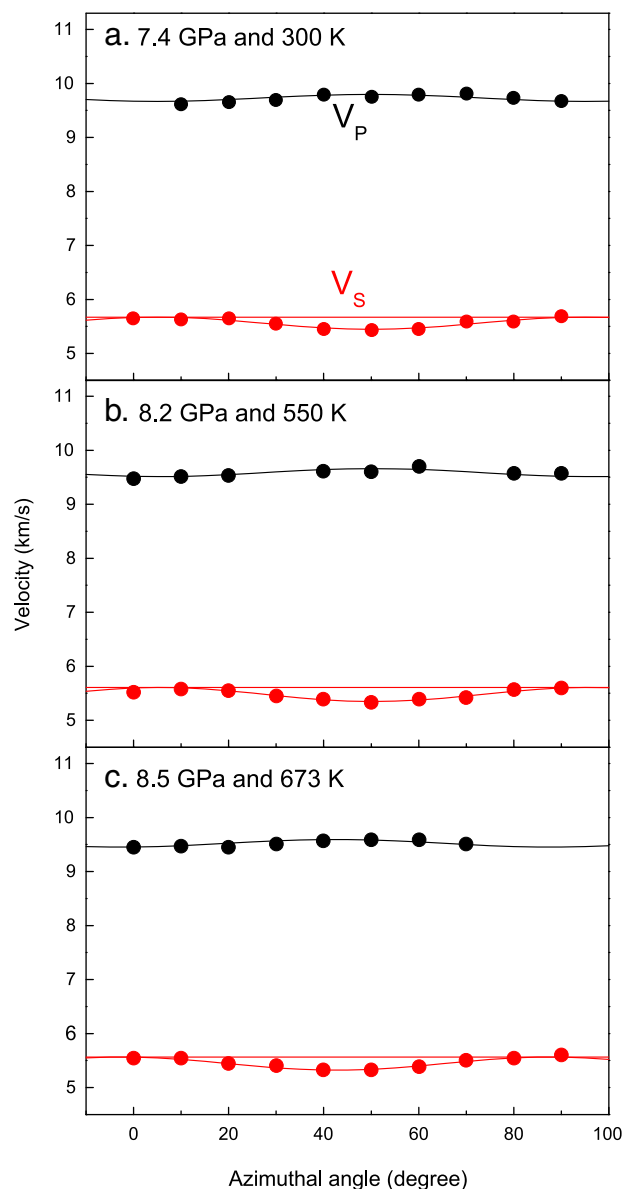


**Fig. 2.** Example of the measured acoustic velocities compared with fitting results. Black and red circles: measured  $V_p$  and  $V_s$ , respectively; black and red lines: fitting results. The two red lines represent two polarized shear waves in our modeling, although only shear wave was observed in this study. (For interpretation of the references to color in this figure legend, the reader is referred to the web version of this article.)

for 60 s. The analysis raster was 7  $\mu\text{m}$  and a beam-blanking mask was used to collect ions from an area of approximately  $2.6 \times 2.6 \mu\text{m}^2$  in the sample at each probe point. The water content was calibrated against three NIST standard silicate glasses, 519–4–4 with 0.17 wt.%  $\text{H}_2\text{O}$ , D52–5 with 1.00 wt.%  $\text{H}_2\text{O}$ , and D30–1 with 1.63 wt.%  $\text{H}_2\text{O}$ . Nine different probe points from rim to rim across one single crystal gave an average water content of  $1.11(\pm 0.06)$  wt.%  $\text{H}_2\text{O}$ , where the reported error is the standard deviation from the mean. Using the measured  $\sum \text{Fe}/(\text{Mg} + \sum \text{Fe})$  from electron microprobe analysis,  $\text{Fe}^{3+}/\sum \text{Fe}$  from Mössbauer spectroscopy, the  $\text{H}_2\text{O}$  content from SIMS, and the lattice parameter from X-ray diffraction, the hydrous ringwoodite sample has a calculated chemical formula of  $(\text{Mg}_{1.633}\text{Fe}^{2+}_{0.231}\text{Fe}^{3+}_{0.026})\text{Si}_{1.00}\text{H}_{0.179}\text{O}_4$  and a density of  $3.649 (\pm 0.003) \text{g/cm}^3$ .

High P–T Brillouin scattering and X-ray diffraction experiments were performed at beamline 13BMD of the GSECARS sector, Advanced Photon Source, Argonne National Laboratory. A single crystal of 30–35  $\mu\text{m}$  thickness was double-side polished and loaded into an externally-heated diamond anvil cell (EHDAC) along with a Ne pressure medium. A Pt foil was placed next to the crystal for in situ pressure measurements, whereas Ne was also used as a secondary pressure calibrant (Fei et al., 2007). A K-type thermocouple, attached onto the diamond 500  $\mu\text{m}$  away from one of the diamond culets, was used for the temperature measurements. Brillouin spectra of hydrous ringwoodite were collected in a forward scattering geometry with  $50^\circ$  scattering angle at pressures up to 16 GPa and three temperatures (300 K, 550 K and 673 K) (Fig. 1). Pressure stability of the EHDAC was monitored by collecting X-ray diffraction patterns after each pressure or temperature increment such that the measured pressure from the pressure calibrant did not change within experimental uncertainties. Pressures were determined from the X-ray diffraction patterns of the Pt calibrant collected before and after each Brillouin measurement. We also collected the diffraction pattern of ringwoodite before and after each heating cycle to determine the unit cell volume and density of the sample. There was no change in the unit cell volume of ringwoodite before and after the heating within experimental uncertainties, indicating that the water content did not change. In addition, Raman spectra were collected from the ringwoodite sample quenched from 673 K and 16 GPa. The vibrational frequencies and spectral intensity in the OH vibrational bands for the quenched sample were similar to those of the starting sample (SFig. 1). We thus conclude that minimal water was lost after the high P–T experiments. This is consistent with previous observations of dehydration of ringwoodite beginning above 720 K (Inoue et al., 2004; Ye et al., 2009).

### 3. Results

Single-crystal elastic constants,  $C_{ij}$ s, of hydrous ringwoodite at each P–T condition were obtained by fitting the measured velocity curves using Christoffel's equation via non-linear least squares methods (Table 1, Figs. 2 and 3) (Every, 1980):

$$|C_{ijkl}n_i n_j - \rho V^2 \delta_{ik}| = 0, \quad (1)$$

where  $C_{ijkl}$  are the elastic constants in full suffix notation,  $n_i$  represents the direction cosines of the phonon propagation direction,  $V$  is the measured acoustic velocity, and  $\rho$  is the averaged density determined by X-ray diffraction before and after the Brillouin scattering measurements at each given P–T condition. The direction cosines of the phonon propagation direction,  $n_i$ , are described by three Eulerian angles ( $\theta, \chi, \varphi$ ). The Eulerian angles relate the laboratory reference to the crystallographic reference frame (Shimizu, 1995), and can be determined from the single-crystal X-ray data.

Using the single-crystal elastic constants, we calculated the Voigt–Reuss–Hill averages for the adiabatic bulk ( $K_{S0} = 175 (\pm 1)$  GPa) and shear ( $G_0 = 106 (\pm 1)$  GPa) moduli (Fig. 4 and Table 1). These results are similar to results from GHz-ultrasonic measurements on similar material, with  $K_{S0} = 177 (\pm 2)$  GPa and  $G_0 = 103 (\pm 1)$  GPa (Jacobsen and Smyth, 2006; Jacobsen et al., 2004). Although the samples from the current Brillouin study (run SZ0104) and the GHz-ultrasonic study (run SZ9901 from Smyth et al., 2003) are both similar in bulk composition and water content, ringwoodite in the current study co-existed with wadsleyite and not stishovite, whereas ringwoodite used in the GHz-ultrasonic measurements (Jacobsen et al., 2004) was made at slightly higher pressures (20 GPa) and co-existed with stishovite and not wadsleyite. The silica activity is known to affect the hydration mechanisms in olivine (Mosenfelder et al., 2006), and it is also possible that there are differences in the defect structure of ringwoodites from these two runs.

At 300 K, third-order finite Eulerian strain equations were used to obtain the pressure derivatives of the elastic moduli, yielding:  $C_{11}' = 6.9 (\pm 0.1)$ ,  $C_{12}' = 2.4 (\pm 0.1)$ ,  $C_{44}' = 1.0 (\pm 0.1)$ ,  $K_{S0}' = 4.0 (\pm 0.1)$ , and  $G_0' = 1.6 (\pm 0.1)$ . However, the longitudinal modulus,  $C_{11}$ , and shear modulus,  $G$ , exhibit a pressure-dependent derivative, and hence they were also fitted to the fourth-order finite Eulerian strain equations (Figs. 3 and 4), yielding  $C_{11}'' = 8.7 (\pm 0.5)$ ,  $C_{11}''' = -0.38 (\pm 0.11) \text{GPa}^{-1}$ ,  $G_0' = 1.98 (\pm 0.2)$ , and  $G_0'' = -0.11 (\pm 0.05) \text{GPa}^{-1}$ .

**Table 1**  
Elastic moduli of hydrous ringwoodite from high P–T Brillouin and X-ray diffraction studies.

Temperature	P (GPa)	$\rho$ ( $\text{g/cm}^3$ )	$C_{11}$ (GPa)	$C_{12}$ (GPa)	$C_{44}$ (GPa)	$K_S$ (GPa)	$G$ (GPa)
300 K	0.0001	3.649(0.003)	299.7(1.7)	112.7(1.8)	115.3(0.5)	175.2(1.3)	106(1.0)
	3.7	3.721(0.003)	328.0(2.0)	122(2.5)	118.5(1.2)	190.7(1.7)	112(1.3)
	5.2	3.753(0.003)	339.1(2.4)	124.6(2.6)	120.3(0.7)	196.1(1.7)	114.9(1.4)
	7.4	3.792(0.003)	354.5(2.3)	129.4(2.4)	122.0(0.6)	204.4(1.7)	118.1(1.3)
	9.0	3.828(0.003)	362.6(2.5)	133.9(2.6)	123.2(0.8)	210.1(1.9)	119.6(1.4)
	10.9	3.855(0.003)	372.2(2.9)	137.6(3.0)	124.9(0.6)	215.8(2.2)	121.8(1.6)
	12.4	3.884(0.003)	380.2(2.0)	142.6(2.7)	125.4(1.1)	221.8(1.9)	122.7(1.4)
550 K	1.6	3.653(0.003)	297.5(2.4)	111.8(2.3)	113.7(0.6)	173.7(1.7)	104.8(1.2)
	5.6	3.734(0.006)	327.5(4.2)	118.5(2.4)	117.2(0.6)	188.2(3.5)	111.9(1.4)
	8.2	3.770(0.003)	341.5(2.5)	125.4(2.6)	118.6(1.0)	197.4(2.0)	114.3(1.4)
	11.7	3.843(0.002)	358.7(1.9)	133.9(2.1)	121.4(0.6)	208.8(1.4)	117.7(1.1)
	13.9	3.883(0.003)	370.8(4.3)	139.9(3.8)	123.0(0.9)	216.9(3.7)	119.9(2.1)
673 K	4.2	3.692(0.002)	312.7(3.2)	112.3(3.7)	112.9(0.6)	179.1(2.9)	107.6(2.0)
	6.5	3.728(0.002)	324.7(2.6)	117.4(2.7)	114.9(0.6)	186.5(2.0)	110.3(1.5)
	8.5	3.768(0.006)	338.6(2.7)	123.3(2.5)	116.7(0.7)	195.1(2.0)	113.0(1.5)
	13.7	3.869(0.002)	362.5(2.8)	136.9(2.9)	121.3(0.8)	212.1(2.2)	117.8(1.6)
	16.3	3.914(0.002)	372.7(4.5)	140.0(5.1)	123.5(0.9)	217.6(4.0)	120.6(2.7)

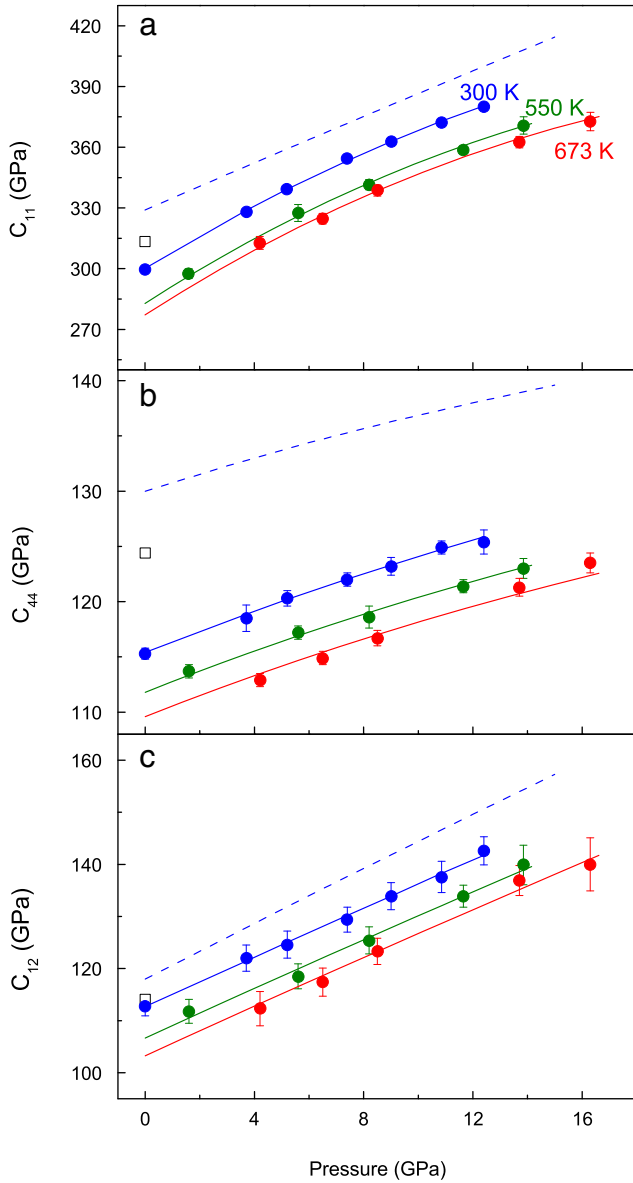


**Fig. 3.** Single-crystal elasticity of hydrous ringwoodite. Blue, green and red circles: measured elasticity of hydrous ringwoodite at 300 K, 550 K and 673 K, respectively; dashed line and open squares: anhydrous  $(\text{Mg}_{0.91}\text{Fe}_{0.09})_2\text{SiO}_4$  ringwoodite at 300 K and 650 K (Sinogeikin et al., 2003), respectively. (For interpretation of the references to color in this figure legend, the reader is referred to the web version of this article.)

The measurements at high temperatures show a similar curvature with increasing pressure at 550 K and 673 K. We conclude that the pressure derivatives of the elastic moduli are similar at high temperature (Figs. 3 and 4). The temperature derivatives of the bulk modulus,  $(\partial K_S/\partial T)_P$ , and shear modulus,  $(\partial G/\partial T)_P$ , at constant pressure were evaluated using a linear equation (Fig. 5). Since  $(\partial K_S/\partial T)_P$  and  $(\partial G/\partial T)_P$  are only slightly affected by pressure, the average value for  $(\partial K_S/\partial T)_P$  and  $(\partial G/\partial T)_P$  over pressure are  $-0.038 (\pm 0.007)$  GPa/K and  $-0.017 (\pm 0.004)$  GPa/K, respectively (Fig. 6).

#### 4. Discussion

The single-crystal elastic constants ( $C_{ij}$ s) and the aggregate bulk ( $K_S$ ) and shear moduli ( $G$ ) of iron-bearing hydrous ringwoodite from analyses of the *in situ* Brillouin and X-ray diffraction measurements show two distinct features: (1) reduced elastic moduli by hydration

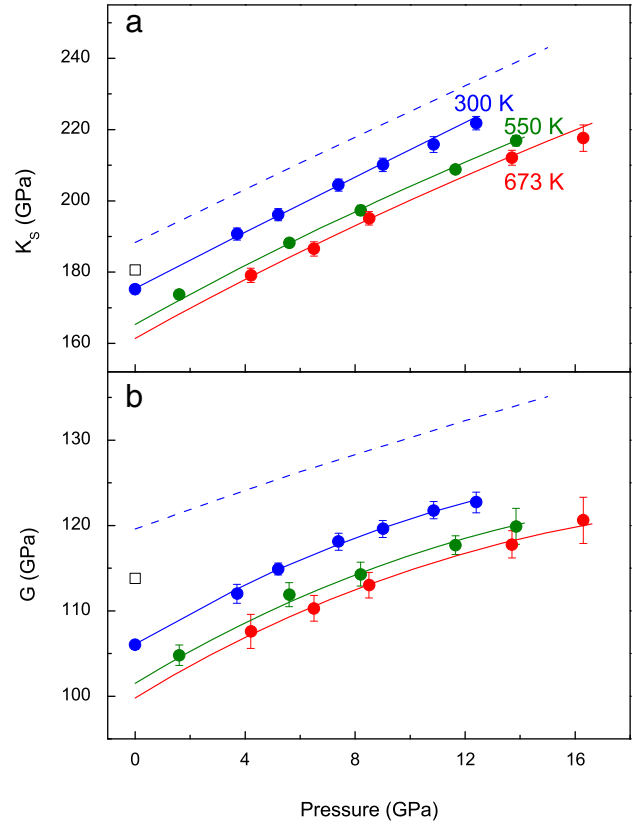


**Fig. 4.** Aggregate bulk ( $K_S$ ) and shear moduli ( $G$ ) of hydrous ringwoodite. Blue, green and red circles:  $K_S$  and  $G$  of hydrous ringwoodite at 300 K, 550 K and 673 K, respectively, in this study; dashed lines and open squares: anhydrous  $(\text{Mg}_{0.91}\text{Fe}_{0.09})_2\text{SiO}_4$  ringwoodite at 300 K and 650 K (Sinogeikin et al., 2003), respectively. (For interpretation of the references to color in this figure legend, the reader is referred to the web version of this article.)

at 300 K comparable to previous GHz-ultrasonic measurements (Jacobsen et al., 2004), and (2) at high pressure, further reduction of elastic moduli at high-temperature (Figs. 3 and 4). As shown in previous studies, hydration reduces the elastic moduli of olivine, wadsleyite and ringwoodite at ambient conditions with the influence of water increasing from olivine to wadsleyite and ringwoodite. In forsterite with about 1 wt.% of water, the pressure derivatives of  $K$  and  $G$  (4.5 and 1.75, respectively) are higher than anhydrous forsterite (4.2–4.4 and 1.4–1.5 from Abramson et al., 1997 and Zha et al., 1996), causing a potential velocity crossover above about 3 GPa at 300 K (Mao et al., 2010). In Fe-free wadsleyite, the pressure derivatives of hydrous wadsleyite are similar to anhydrous wadsleyite (Mao et al., 2008b) (STable 1). Fe-bearing hydrous wadsleyite (Fo90) containing 2 wt.%  $\text{H}_2\text{O}$  displays similar  $K'$  (4.8) to anhydrous wadsleyite (4.6–4.7) but a higher  $G'$  (1.9) compared with anhydrous Fe-bearing wadsleyite (1.5) (Mao et al., 2011) (STable 1). In contrast to a previous high-pressure, GHz-ultrasonic study of hydrous Fe-bearing ringwoodite, which showed an increase in the pressure derivatives of both  $K$  (5.3) and  $G$  (2.0) (Jacobsen and Smyth, 2006), here we find that the  $K'$  and  $G'$  of Fe-bearing hydrous ringwoodite are similar to anhydrous Fe-bearing ringwoodite. The discrepancy between the current pressure derivatives of Fe-bearing hydrous ringwoodite from the high-pressure GHz-ultrasonic study of Jacobsen and Smyth (2006) is not yet understood, but it could possibly result from different hydration mechanisms (Panero, 2010) between the two samples synthesized under different conditions (run SZ0401 and run SZ9901 of Smyth et al., 2003) or it is possible that the silica gel introduced into the GHz-ultrasonic study hardened at high pressure causing a uniaxial stress on the sample in the direction of the acoustic wave propagation. We note that the static

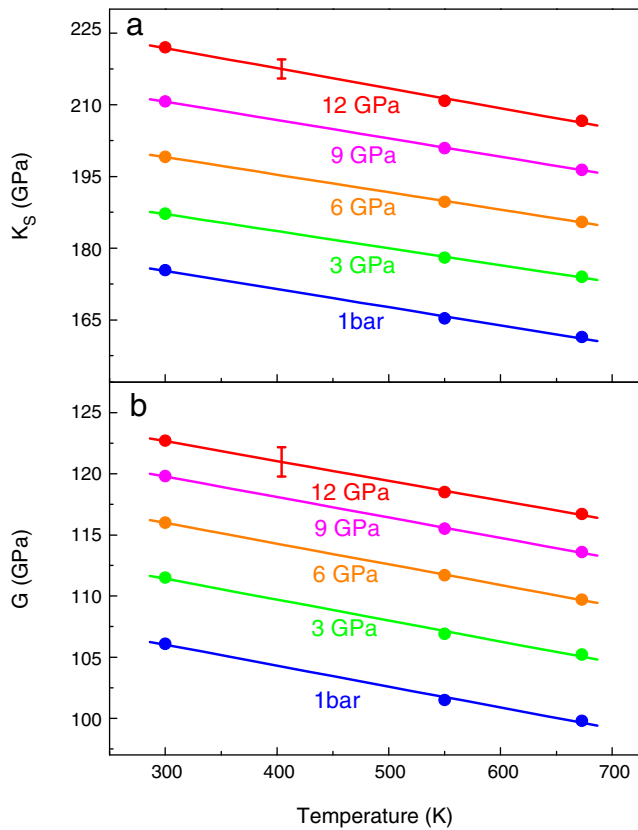


**Fig. 5.** Effect of temperature on the bulk,  $K_S$ , and shear moduli,  $G$ , of hydrous ringwoodite at a given pressure. A linear fit was applied to obtain the temperature derivative of  $K_S$  and  $G$ . Vertical lines represent the propagated uncertainties ( $\pm 1\sigma$ ).

compression study of Fe-bearing hydrous ringwoodite of Manghni et al. (2005) reported a similarly high derivative of the bulk modulus with  $K' = 6.2$ . However, if the pressure derivatives of the moduli in hydrous phases are similar to anhydrous phases, as evidenced from the current study, the same amount of water in Fe-bearing ringwoodite can produce two to three times reductions in the elastic moduli compared to those of wadsleyite and olivine at high pressures because the initial (low pressure) moduli are more reduced in ringwoodite than in wadsleyite or olivine. Our experiments showed that all of the elastic moduli of hydrous ringwoodite exhibit similar pressure derivatives as compared to the anhydrous counterparts, but the addition of 1.1 wt.%

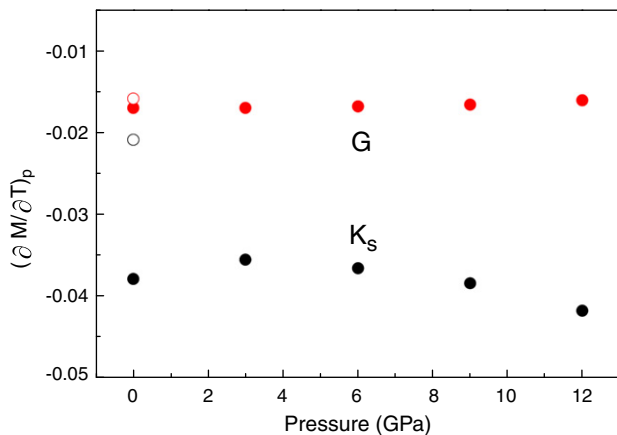


**Fig. 6.** Temperature derivative of the bulk (black) and shear moduli (red). Solid circles: hydrous ringwoodite, this study; open circles: anhydrous ringwoodite (Sinogeikin et al., 2003). (For interpretation of the references to color in this figure legend, the reader is referred to the web version of this article.)

$H_2O$  lowers these constants by 5–9% at high pressures and high temperatures (Figs. 3 and 4).

High temperatures further reduce the elastic moduli of hydrous ringwoodite at high pressures (compared with anhydrous ringwoodite) but does not have a noticeable effect on their pressure derivatives (Figs. 3 and 4). Specifically, increasing temperature by 100 K would decrease the elastic moduli of hydrous ringwoodite by 1.3–2.4% at 12 GPa, much greater than the observed 0.5–1.2% reduction for anhydrous ringwoodite (Figs. 3 and 4) (Sinogeikin et al., 2003). The bulk modulus is more sensitive to temperature than the shear modulus; the temperature derivative of  $K_S$  is  $-0.038 (\pm 0.007)$  GPa/K, much greater than that of anhydrous ringwoodite ( $-0.021 (\pm 0.002)$  GPa/K) (Figs. 3, 4, and 6) (Higo et al., 2008; Mayama et al., 2005; Sinogeikin et al., 2003). The strong reduction in the elastic moduli of hydrous ringwoodite reflects a net effect of temperature, iron content, and hydration mechanism in our samples.

Next we modeled the sound velocity of ringwoodite using a thermal Birch–Murnaghan equation of state and our experimental results (Figs. 7 and 8) (Duffy and Anderson, 1989). Based on these calculations, the presence of ~1 wt.%  $H_2O$  in ringwoodite causes an approximate 2.5 ( $\pm 0.4$ )% reduction in the compressional ( $V_P$ ) and shear ( $V_S$ ) velocities at 300 K at a depth between 520 and 660 km. The velocity reduction is approximately two times more than that in Fe-bearing wadsleyite with 2 wt.%  $H_2O$  (Fig. 8) (Mao et al., 2011). Since the wadsleyite-to-ringwoodite transition is expected to occur at approximately 520-km depth, our findings indicate that seismic wave velocities at 520 to 660-km depth may be more sensitive to hydration than the layer above (Jacobsen et al., 2008; Mao et al., 2008a,b, 2010, 2011). Considering the overall effect of iron content, hydration and temperature, our model further shows that the  $V_P$  and  $V_S$  of hydrous ringwoodite along a mantle geotherm are 7 ( $\pm 0.5$ )% and 4.5 ( $\pm 0.7$ )% lower than those of the anhydrous ringwoodite (Fig. 8); these differences could be further enhanced by anelasticity effects (Karato, 1995), which need to be taken into account in future studies.

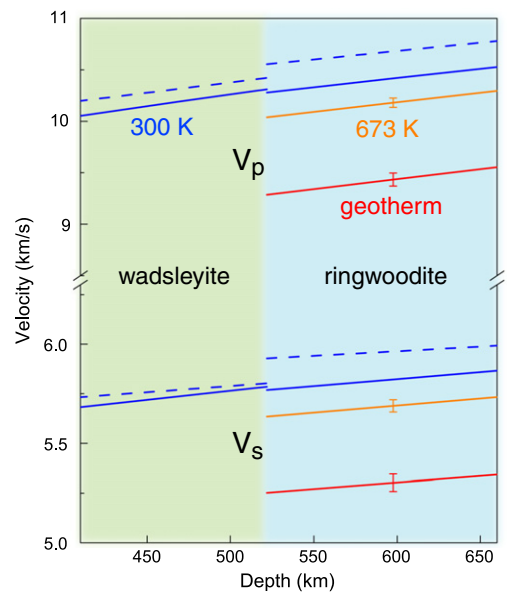


**Fig. 7.** Modeled  $V_P$  and  $V_S$  of ringwoodite in the transition zone. Blue dashed line: anhydrous ringwoodite (wadsleyite) at 300 K (Sinogeikin et al., 2003; Liu et al., 2009); solid line: ringwoodite with 1.1 wt.%  $H_2O$  at 300 K (blue), 673 K (orange) and along the 1400 °C mantle geotherm (red) and wadsleyite with 2 mol%  $H_2O$  (blue) (Mao et al., 2011). Vertical lines represent the propagated uncertainties ( $\pm 1\sigma$ ). (For interpretation of the references to color in this figure legend, the reader is referred to the web version of this article.)

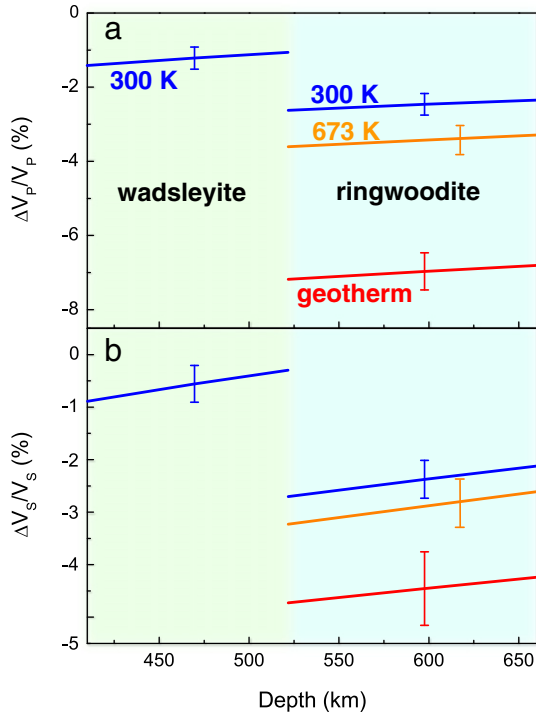


**Fig. 8.** Effect of hydration on the sound velocity of ringwoodite. Blue, orange and red lines for ringwoodite with 1 wt.% H<sub>2</sub>O: at 300 K, 673 K and along the mantle geotherm (1400 °C); blue line for hydrous wadsleyite with 2 wt.% H<sub>2</sub>O: at 300 K (Mao et al., 2011). Vertical lines represent the propagated uncertainties ( $\pm 1\sigma$ ). (For interpretation of the references to color in this figure legend, the reader is referred to the web version of this article.)

Quantifying the amount of H<sub>2</sub>O in the Earth's mantle has been a long-standing challenge in deep-Earth research integrating seismology, mineral physics, and geodynamics. Using the measured sound velocities of hydrous ringwoodite at simultaneous high P–T, our results can be applied to interpreting seismic signatures in the potential water-rich region of the transition zone where ringwoodite is believed to be the most abundant phase. Seismic velocity anomalies, together with the depth depression of the 660-km discontinuity at the bottom part of the transition zone in regions near subducting slabs are expected to reflect potential regions of hydration. Recent experimental studies have shown that the presence of water can displace the 660-km discontinuity to deeper depths (Higo et al., 2001), similar to the effect of cold subducting slabs, and lower the seismic velocity (Jacobsen and Smyth, 2006; Wang et al., 2003, 2006). The observed anomalies in depth and velocity in the regions are thus expected to be the cause of combined water and temperature effects.

Based on recent seismic studies, the 660-km discontinuity exhibits a depth depression of 10–40 km, with a 0.3%–3% anomaly in  $V_p$  and 1–2% in  $V_s$  in the subduction areas beneath the Japan and Philippine sea, Caribbean–South American Plate boundary, and western United States (Cao and Levander, 2010; Flanagan and Shearer, 1998; Fukao et al., 2001, 2009; Grand, 2002; Houser et al., 2008; Mégnin and Romanowicz, 2000; Niu et al., 2005; Suetsugu et al., 2006, 2010; Tono et al., 2005; van der Lee et al., 2008; Widiyantoro et al., 1999). Using the depth depression of the 660-km discontinuity and associated velocity anomalies from seismic observations, water content in related regions can be estimated as follows (Suetsugu et al., 2006):

$$\delta d = \frac{\partial d}{\partial T} \delta T + \frac{\partial d}{\partial W} \delta W, \quad (2)$$

$$\delta V = \frac{\partial V}{\partial T} \delta T + \frac{\partial V}{\partial W} \delta W, \quad (3)$$

where  $\delta d$  is the depression on the depth of the 660-km discontinuity,  $\delta V$  is the observed seismic velocity anomaly, and  $W$  is the water content. Here we only consider the first-order temperature and water derivatives of velocity (depth), respectively. The water content and the temperature anomalies at the bottom part of the transition zone were determined using the following literature values: (1)  $\partial V/\partial W$ , the effect of water on the velocity, determined in this study; (2)  $\partial d/\partial T$ , the effect of temperature on the depth of the 660-km discontinuity, is  $-0.06$  km/K as derived from the Clapeyron slope of the phase transition from ringwoodite to perovskite and ferropericlase (Akaogi and Ito, 1993; Bina and Helffrich, 1994; Fei et al., 2004; Higo et al., 2001; Irifune and Isshiki, 1998; Katsura et al., 2003; Litasov et al., 2005); (3)  $\partial d/\partial W$ , the effect of hydration on the depth of the 660-km discontinuity, is 6 km/wt.% (Higo et al., 2001; Lee et al., 2005); (4)  $\partial V/\partial T$ , the temperature dependence on  $V_p$  ( $-3.8 \times 10^{-4}$  km/K) or  $V_s$  of ringwoodite ( $-3.0 \times 10^{-4}$  km/K) (Sinogeikin et al., 2003).

Using Eqs. (2) and (3), we estimated the water content and temperature anomalies at the bottom of the transition zone near subducted slabs (Fig. 9). Since the P-wave travel-time spectra have higher resolution to image the stagnant slabs than the S-wave spectra, we focused on using the P-wave data to estimate the water content in the region. Thus, water content estimated from the  $V_p$  anomalies and the depth depression of the 660-km discontinuity is less than  $0.1 (\pm 0.2)$  wt.% in the related regions, where estimated temperature anomalies are approximately 200–500 K (Fig. 9). The amount of water estimated here is three to five times less than that predicted in previous work, without considering the net effect of water and temperature (Cao and Levander, 2010; Houser et al., 2008; Suetsugu et al., 2010). The water content estimated here for the lowest portion of the Earth's transition zone is consistent with recent studies using seismicity (Green et al., 2010), electromagnetic induction (Kelbert et al., 2009),

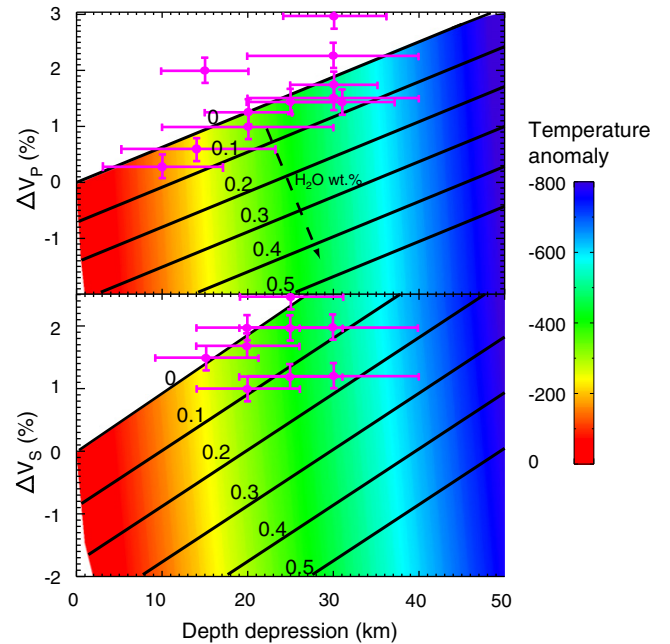


**Fig. 9.** Water and temperature anomalies at the bottom of the transition zone (660-km depth). Contour: water content; colored bar: temperature anomalies; pink circles: the water and temperature anomalies needed to explain the seismic observations in the subducting slabs and the surrounding mantle under Japan, Philippine sea, Izu-Bonin, South American and Western United at the bottom of the transition zone (Cao and Levander, 2010; Flanagan and Shearer, 1998; Fukao et al., 2001, 2009; Grand, 2002; Houser et al., 2008; Mégnin and Romanowicz, 2000; Niu et al., 2005; Suetsugu et al., 2006, 2010; Tono et al., 2005; Widiyantoro et al., 1999). (For interpretation of the references to color in this figure legend, the reader is referred to the web version of this article.)

and electronic conductivity of wadsleyite and ringwoodite (Yoshino et al., 2008).

Our results here confirm the idea that the presence of water can lower the elasticity and sound velocities of mantle minerals. However, the magnitude of the reduction by a given amount of water is much greater than previously thought, when the combined effect of hydration, temperature, and pressure is taken into consideration. Specifically, hydration strongly increases the magnitude of the temperature derivative of the bulk modulus. Compared to previous ultrasonic and static compression (X-ray diffraction) studies, the increased temperature derivatives lead to an enhanced reduction in the sound velocity by hydration at high pressures. Ignoring the combined effect of hydration, temperature, and pressure can thus lead to an overestimation of the mantle water budget. In addition, the effect of hydration on the elasticity of other major mantle phases, including garnet and pyroxene, also needs to be taken into account in future studies evaluating the potential mantle H<sub>2</sub>O content.

## Acknowledgments

We thank I. Kantor and K. K. Zhuravlev for experimental assistance and A. Wheat for manuscript editing. Experiments performed at GeoSoilEnviroCARS (Sector 13), Advanced Photon Source (APS), Argonne National Laboratory, was supported by the National Science Foundation (NSF) through EAR-0622171 and U.S. Department of Energy (DE-FG02-94ER14466). Use of the Advanced Photon Source was supported by the DOE, Office of Science, Office of Basic Energy Sciences, under Contract No. DE-AC02-06CH11357. Support for Brillouin scattering and gas loading equipment was provided by GSE-CARS and COMPRES, the Consortium for Materials Properties Research in Earth Sciences under NSF Cooperative Agreement EAR 10-43050. This research was supported by the NSF grants EAR-0838221 and EAR-1056670 to J.F. Lin, EAR-0748707 to S.D. Jacobsen, EAR-0738510 to T.S. Duffy, and EAR07-11165 and 11-13369 to J.R. Smyth. Additional support was provided by the Carnegie/DOE Alliance Center (CDAC) and Energy Frontier Research in Extreme Environments (EFree) to J.F. Lin, and by the David and Lucile Packard Foundation to S.D. Jacobsen.

## Appendix A. Supplementary data

Supplementary data to this article can be found online at doi:10.1016/j.epsl.2012.03.001.

## References

Abramson, E.H., Brown, J.M., Slutsky, L.J., Zaug, J., 1997. The elastic constants of San Carlos olivine to 17 GPa. *J. Geophys. Res.* 102, 12,253–12,263.

Akaogi, M., Ito, E., 1993. Heat capacity of MgSiO<sub>3</sub> perovskite. *Geophys. Res. Lett.* 20, 105–108.

Bercovici, D., Karato, S., 2003. Whole-mantle convection and the transition zone water filter. *Nature* 425, 39–44.

Bina, C.R., Helffrich, G., 1994. Phase transition Clapeyron slopes and transition zone seismic discontinuity topography. *J. Geophys. Res.* 99, 15853–15860.

Braunmiller, J., van der Lee, S., Doermann, L., 2006. Mantle transition zone thickness in the central South-American subduction zone. In: Jacobsen, S.D., van der Lee, S. (Eds.), *Earth's Deep Water Cycle*. American Geophysical Union, Washington, D. C., pp. 215–224.

Cao, A., Levander, A., 2010. High-resolution transition zone structures of the Gorda Slab beneath the western United States: implication for deep water subduction. *J. Geophys. Res.* 115, B07301.

Chen, J., Inoue, T., Weidner, D.J., Wu, Y.J., Vaughan, M.T., 1998. Strength and water weakening of mantle minerals, olivine, wadsleyite and ringwoodite. *Geophys. Res. Lett.* 25, 575–578.

Courtier, A.M., Revenaugh, J., 2006. A water-rich transition zone beneath the eastern United States and Gulf of Mexico from multiple ScS reverberations. In: Jacobsen, S.D., van der Lee, S. (Eds.), *Earth's Deep Water Cycle*. American Geophysical Union, Washington, D. C., pp. 181–193.

Courtier, A.M., Revenaugh, J., 2007. Deep upper-mantle melting beneath the Tasman and Coral Seas detected with multiple ScS reverberations. *Earth Planet. Sci. Lett.* 259, 66–76.

Duffy, T.S., Anderson, D.L., 1989. Seismic velocities in mantle minerals and the mineralogy of the upper mantle. *J. Geophys. Res.* 94, 1895–1912.

Every, A.G., 1980. General closed-form expressions for acoustic waves in elastically anisotropic solids. *Phys. Rev. B* 22, 1746–1760.

Fei, Y., Van Orman, J., Li, J., van Westrenen, W., Sanloup, C., Minarik, W., Hirose, K., Komabayashi, T., Walter, M., Funakoshi, K., 2004. Experimentally determined postspinel transformation boundary in Mg<sub>2</sub>SiO<sub>4</sub> using MgO as an internal pressure standard and its geophysical implication. *Phys. Earth Planet. Inter.* 109, B02305.

Fei, Y., Ricolleau, A., Frank, M., Mibe, K., Shen, G., Prakapenka, V., 2007. Towards an internally consistent pressure scale. *Proc. Natl. Acad. Sci. U. S. A.* 104, 9182–9186.

Flanagan, M.P., Shearer, P.M., 1998. Global mapping of topography on transition zone velocity discontinuities by stacking SS precursors. *J. Geophys. Res.* 103, 2673–2692.

Frost, D.J., Dolejš, D., 2007. Experimental determination of the effect of H<sub>2</sub>O on the 410-km seismic discontinuity. *Earth Planet. Sci. Lett.* 256, 182–195.

Fukao, Y., Widiyantoro, S., Obayashi, M., 2001. Stagnant slabs in the upper and lower mantle transition zone. *Rev. Geophys.* 39, 91–323.

Fukao, Y., Obayashi, M., Nakakuki, T., the Deep Slab Project Group, 2009. Stagnant slab: a review. *Annu. Rev. Earth Planet. Sci.* 37, 19–46.

Grand, S.P., 2002. Mantle shear-wave tomography and the fate of subducted slabs. *Philos. Trans. R. Soc. Lond. A* 360, 2475–2491.

Green, H.W., Chen, W.-P., Brudzinski, M.R., 2010. Seismic evidence of negligible water carried below 400-km depth in subducting lithosphere. *Nature* 467, 828–831.

Higo, Y., Inoue, T., Yurimoto, H., 2001. Effect of water on spinel–postspinel transformation in Mg<sub>2</sub>SiO<sub>4</sub>. *Geophys. Res. Lett.* 28, 3505–3508.

Higo, Y., Inoue, T., Irifune, T., Funakoshi, K.-I., Li, B., 2008. Elastic wave velocities of (Mg<sub>0.91</sub>Fe<sub>0.09</sub>)<sub>2</sub>SiO<sub>4</sub> ringwoodite under P–T conditions of the mantle transition region. *Phys. Earth Planet. Inter.* 166, 167–174.

Hirschmann, M.M., 2006. Water, melting, and the deep Earth H<sub>2</sub>O cycle. *Annu. Rev. Earth Planet. Sci.* 34, 629–653.

Houser, C., Masters, G., Flanagan, M.P., Shearer, P.M., 2008. Determination and analysis of long-wavelength transition zone structure using SS precursors. *Geophys. J. Int.* 174, 178–194.

Huang, X.G., Xu, Y.S., Karato, S., 2005. Water content in the transition zone from electrical conductivity of wadsleyite and ringwoodite. *Nature* 434, 746–749.

Inoue, T., Tanimoto, Y., Irifune, T., Suzuki, T., Fukui, H., Ohtaka, O., 2004. Thermal expansion of wadsleyite, ringwoodite, hydrous wadsleyite and hydrous ringwoodite. *Phys. Earth Planet. Inter.* 143–144, 279–290.

Inoue, T., Wada, T., Sasaki, R., Yurimoto, H., 2010. Water partitioning in the Earth's mantle. *Phys. Earth Planet. Inter.* 183, 245–251.

Irifune, T., Isshiki, M., 1998. Iron partitioning in a pyrolite mantle and the nature of the 410-km seismic discontinuity. *Nature* 392, 702–705.

Jacobsen, S.D., 2006. Effect of water on the equation of state of nominally anhydrous minerals. *Rev. Mineral. Geochem.* 62, 321–342.

Jacobsen, S.D., Smyth, J.R., 2006. Effect of water on the sound velocities of ringwoodite in the transition zone. In: Jacobsen, S.D., van der Lee, S. (Eds.), *Earth's Deep Water Cycle*. American Geophysical Union, Washington, D. C., pp. 131–145.

Jacobsen, S.D., Smyth, J.R., Spetzler, H., Holl, C.M., Frost, D.J., 2004. Sound velocities and elastic constants of iron-bearing hydrous ringwoodite. *Phys. Earth Planet. Inter.* 143–144, 47–56.

Jacobsen, S.D., Jiang, F., Mao, Z., Duffy, T.S., Smyth, J.R., Holl, C.M., Frost, D.J., 2008. Effects of hydration on the elastic properties of olivine. *Geophys. Res. Lett.* 35, L14303.

Jasbinsek, J.J., Dueker, K.G., Hansen, S.M., 2010. Characterizing the 410 km discontinuity low-velocity layer beneath the LA RISTRA array in the North American Southwest. *Geochem. Geophys. Geosyst.* 11, Q03008.

Karato, S., 1995. Effects of water on seismic wave velocities in the upper mantle. *Proc. Jpn. Acad.* 71, 61–66.

Katsura, T., Yamada, H., Shinmei, T., Kubo, A., Ono, S., Kanzaki, M., Yoneda, A., Walter, M.J., Ito, E., Urakawa, S., Funakoshi, K., Utsumi, W., 2003. Post-spinel transition in Mg<sub>2</sub>SiO<sub>4</sub> determined by high P–T in situ X-ray diffractometry. *Phys. Earth Planet. Inter.* 136, 11–24.

Kawakatsu, H., Watada, S., 2007. Seismic evidence for deep water transportation in the mantle. *Science* 316, 1468–1471.

Kawakatsu, H., Yoshioka, S., 2011. Metastable olivine wedge and deep dry cold slab beneath SW Japan. *Earth Planet. Sci. Lett.* 303, 1–10.

Kelbert, A., Schultz, A., Egbert, G., 2009. Global electromagnetic induction constraints on transition-zone water content variations. *Nature* 460, 1003–1007.

King, H.E., Finger, L.W., 1979. Diffracted beam crystal centering and its application to high-pressure crystallography. *J. Appl. Crystallogr.* 12, 374–378.

Kohlstedt, D.L., Keppler, H., Rubie, D.C., 1996. Solubility of water in the  $\alpha$ ,  $\beta$ , and  $\gamma$  phases of (Mg, Fe)<sub>2</sub>SiO<sub>4</sub>. *Contrib. Mineral. Petrol.* 123, 345–357.

Lee, C.-T.A., Lenardic, A., Cooper, C.M., Niu, F., Levander, A., 2005. The role of chemical boundary layers in regulating the thickness of continental and oceanic thermal boundary layers. *Earth Planet. Sci. Lett.* 230, 379–395.

Lin, L., Du, J., Zhao, J., Liu, H., Gao, H., Chen, Y., 2009. Elastic properties of hydrous forsterites under high pressure: first-principle calculations. *Phys. Earth Planet. Inter.* 176, 89–97.

Litasov, K.D., Ohtani, E., Sano, A., Suzuki, A., 2005. Wet subduction versus cold subduction. *Geophys. Res. Lett.* 32, L13312.

Manghnani, M.H., Amulele, G., Smyth, J.R., Holl, C.M., Chen, G., Prakapenka, V., Frost, D.J., 2005. Equation of state of hydrous Fo90 ringwoodite to 45 GPa by synchrotron powder diffraction. *Mineral. Mag.* 69, 317–323.

Mao, Z., Jacobsen, S.D., Jiang, F., Smyth, J.R., Holl, C., Frost, D.J., Duffy, T.S., 2008a. Single-crystal elasticity of wadsleyites,  $\beta$ -Mg<sub>2</sub>SiO<sub>4</sub>, containing 0.37–1.66 wt.% H<sub>2</sub>O. *Earth Planet. Sci. Lett.* 268, 540–549.

- Mao, Z., Jacobsen, S.D., Jiang, F., Smyth, J.R., Holl, C.M., Duffy, T.S., 2008b. Elasticity of hydrous wadsleyite to 12 GPa: implications for Earth's transition zone. *Geophys. Res. Lett.* 35, L21305. doi:10.1029/2008GL035618.
- Mao, Z., Jacobsen, S.D., Jiang, F., Smyth, J.R., Holl, C., Frost, D.J., Duffy, T.S., 2010. Velocity crossover between hydrous and anhydrous forsterite at high pressures. *Earth Planet. Sci. Lett.* 293, 250–258.
- Mao, Z., Jacobsen, S.D., Frost, D.J., C. A. McCammon, Hauri, E.H., Duffy, T.S., 2011. Effect of hydration on the single-crystal elasticity of Fe-bearing wadsleyite to 12 GPa. *Am. Mineral.* 96, 1606–1612.
- Mayama, N., Suzuki, I., Saito, T., Ohno, I., Katsura, T., Yoneda, A., 2005. Temperature dependence of the elastic moduli of ringwoodite. *Phys. Earth Planet. Inter.* 148, 353–359.
- Mégnin, C., Romanowicz, B., 2000. The three-dimensional shear velocity structure of the mantle from the inversion of body, surface and higher-mode waveforms. *Geophys. J. Int.* 143, 709–728.
- Mosenfelder, J.L., Delinge, N.I., Asimow, P.D., Rossman, G.R., 2006. Hydrogen incorporation in olivine from 2–12 GPa. *Am. Mineral.* 91, 285–294.
- Niu, F., Levander, A., Ham, S., Obayashi, M., 2005. Mapping the subducting Pacific slab beneath southwest Japan with. *Earth Planet. Sci. Lett.* 239, 9–17.
- Nolet, G., Zielhuis, A., 1994. Low S velocities under the Tornquist–Teisseyre zone: evidence for water injection into the transition zone by subduction. *Geophys. Res. Lett.* 99, 15,813–15,820.
- Ohtani, E., 2005. Water in the mantle. *Elements* 1, 25–30.
- Panero, W.R., 2010. First principles determination of the structure and elasticity of hydrous ringwoodite. *J. Geophys. Res.* 115, B03203.
- Shimizu, H., 1995. High-pressure Brillouin scattering of molecular single-crystals grown in a diamond-anvil cell. In: Senoo, M., Suito, K., Kobayashi, T., Kubota, H. (Eds.), *High Pressure Research on Solids*. Elsevier, Netherlands, pp. 1–17.
- Sinogeikin, S.V., Bass, J.D., Katsura, T., 2003. Single-crystal elasticity of ringwoodite to high pressures and high temperatures: implications for 520 km seismic discontinuity. *Phys. Earth Planet. Inter.* 136, 41–66.
- Smyth, J.R., 1987.  $\beta$ -Mg<sub>2</sub>SiO<sub>4</sub>: a potential host for water in the mantle? *Am. Mineral.* 72, 1051–1055.
- Smyth, J.R., Jacobsen, S.D., 2006. Nominally anhydrous minerals and earth's deep water cycle. In: Jacobsen, S.D., van der Lee, S. (Eds.), *Earth's Deep Water Cycle*. American Geophysical Union, Washington, D. C., pp. 1–11.
- Smyth, J.R., Holl, C.M., Frost, D.J., Jacobsen, S.D., Langenhorst, F., McCammon, C.A., 2003. Structural systematics of hydrous ringwoodite and water in Earth's interior. *Am. Mineral.* 88, 1402–1407.
- Song, T.A., Helmlinger, D.V., Grand, S.P., 2004. Low-velocity zone atop the 410-km seismic discontinuity in the northwestern United States. *Nature* 427, 530–533.
- Suetsugu, D., Inoue, T., Yamada, A., Zhao, D., Obayashi, M., 2006. Towards mapping the three-dimensional distribution of water in the transition zone from P-velocity tomography and 660-km discontinuity depths. In: Jacobsen, S.D., van der Lee, S. (Eds.), *Earth's Deep Water Cycle*. American Geophysical Union, Washington, D. C., pp. 237–250.
- Suetsugu, D., Inoue, T., Obayashi, M., Yamada, A., Shiobara, H., Sugioka, H., Ito, A., Kanazawa, T., Kawakatsu, H., Shito, A., Fukao, Y., 2010. Depths of the 410-km and 660-km discontinuities in and around the stagnant slab beneath the Philippine Sea: is water stored in the stagnant slab? *Earth Planet. Sci. Lett.* 183, 270–279.
- Tono, Y., Kunugi, T., Fukao, Y., Tsuboi, S., Kanjo, K., 2005. Mapping of the 410- and 660-km discontinuities beneath the Japanese islands. *J. Geophys. Res.* 110, B03307.
- Tsuchiya, J., Tsuchiya, T., 2009. First principles investigation of the structural and elastic properties of hydrous wadsleyite under pressure. *J. Geophys. Res.* 114, B02206.
- van der Lee, S., Regenauer-Lieb, K., Yuen, D.A., 2008. The role of water in connecting past and future episodes of subduction. *Earth Planet. Sci. Lett.* 273, 15–27.
- van der Meijde, M., Marone, F., Giardini, D., van der Lee, S., 2003. Seismic evidence for water deep in earth's upper mantle. *Science* 300, 1556–1558.
- Wang, J., Sinogeikin, S.V., Inoue, T., Bass, J.D., 2003. Elastic properties of hydrous ringwoodite. *Am. Mineral.* 88, 1608–1611.
- Wang, J., Sinogeikin, S.V., Inoue, T., Bass, J.D., 2006. Elastic properties of hydrous ringwoodite at high-pressure conditions. *Geophys. Res. Lett.* 33, L14308. doi:10.1029/2006GL026441.
- Widiyantoro, S., Kennett, B.L.N., van der Hilst, R.D., 1999. Seismic tomography with P and S data reveals lateral variations in the rigidity of deep slabs. *Earth Planet. Sci. Lett.* 173, 91–100.
- Williams, Q., Hemley, R.J., 2001. Hydrogen in the deep earth. *Annu. Rev. Earth Planet. Sci.* 29, 365–418.
- Ye, Y., Schwing, R.A., Smyth, J.R., 2009. Effects of hydration on thermal expansion of forsterite, wadsleyite, and ringwoodite at ambient pressure. *Am. Mineral.* 94, 899–904.
- Yoshino, T., Mantilake, G., Matsuzaki, T., Katsura, T., 2008. Dry mantle transition zone inferred from the conductivity of wadsleyite and ringwoodite. *Nature* 451, 326–329.
- Zha, C.S., Duffy, T.S., Downs, R.T., Mao, H.K., Hemley, R.J., 1996. Sound velocity and elasticity of single-crystal forsterite to 16 GPa. *J. Geophys. Res.* 101, 17,535–17,545.